Univerzita Komenského v Bratislave
Fakulta matematiky fyziky a informatiky

Mgr. Martin Hurban

Autoreferát dizertačnej práce

Convection in multicomponent systems

na získanie akademického titulu *philosophiae doctor*

v odbore doktorandského štúdia:

9.1.9. Aplikovaná matematika

Bratislava 2019

Dizertačná práca bola vypracovaná:
v dennej forme doktorandského štúdia na Katedre aplikovanej matematiky a štatistiky Fakulty matematiky, fyziky a informatiky Univerzity Komenského v Bratislave.

Predkladateľ: Mgr. Martin Hurban
Katedra aplikovanej matematiky a štatistiky
Fakulta matematiky, fyziky a informatiky
Univerzita Komenského v Bratislave
Mlynská dolina
842 48 Bratislava

Školiteľ: doc. Mgr. Peter Guba, PhD.
Katedra aplikovanej matematiky a štatistiky
Fakulta matematiky, fyziky a informatiky
Univerzita Komenského v Bratislave
Mlynská dolina
842 48 Bratislava

Obhajoba dizertačnej práce sa koná ..... o ..... h
pred komisiou pre obhajobu dizertačnej práce v odbore doktorandského štúdia
vymenovanou predsedom odborovej komisie dňa .....
v študijnom odbore 9.1.9. Aplikovaná matematika
na Fakulte matematiky, fyziky a informatiky Univerzity Komenského v Bratislave,
Mlynská dolina, 842 48 Bratislava

Predseda odborovej komisie:
prof. RNDr. Marek Fila, DrSc.
Katedra aplikovanej matematiky a štatistiky
Fakulta matematiky, fyziky a informatiky
Univerzita Komenského v Bratislave
Mlynská dolina
842 48 Bratislava

1 Introduction

Phase change is a phenomenon which occurs on different scales and in various fields. In nature, the processes involving solidification are present in the Earth's core [8], the shelf ice formation [18] or the sediment formation from magma [1], for a recent review, see [4]. A reverse process of solidification (melting and dissolution) can be observed as thawing of permafrost [9]. Apart from nature, there are direct applications in industry such as casting deformity prediction in metallurgy [6] and the modelling of cell cryopreservation in biology [5]. The solidification problems can be formulated within the framework of partial differential equations with a moving boundary of infinitesimally small thickness [7].

During solidification of a pure material, the solid–liquid interface may become thermally supercooled, which enables nucleation as heat is removed from the interfacial regions by convection or conduction (or both). In the case of solidifying a mixture of two or more components, the solidification interface may be exposed to constitutional supercooling, which is caused by segregation of solute into the liquid region. Rejected solute will lower the melting point in the boundary layer of the liquid, thus widening the freezing range of the alloy. This effect (see e. g. [17]) causes the solidifying interface to become morphologically unstable, giving rise to the formation of dendrites. Regions containing liquid and solid phases with dendritic structure are called mushy regions (see [23] or [4]).

1.1 Lateral directional solidification

A setup related to experimental continuous spin casting processes was analysed in [16] and [14]. The two-dimensional boundary layer flow and solidification of a binary alloy over a horizontally moving plate maintained at constant temperature was analysed. A novel feature that distinguishes this setting from the fixed-plate setups is the occurrence of a non-planar interface between the solid and liquid regions.

The model presented in [15] (the original contribution of the author of this thesis) includes liquid, mushy and solid layers and identifies two-dimensional steady self-similar solutions for the system. The effects of boundary flow on the position of the interfaces and solidification speed were quantified. An asymptotic analysis of the parametric dependence of the characteristics of the solidifying system was performed. A comparison to the case of solidification from a cooled boundary analysed in [22] showed that the formation of a

mushy layer in the present setup was more prominent. A generalized model containing two different mushy zones, dispersed and packing, was analysed in [20].

1.2 Vertical directional solidification

Directional solidification of binary mixtures is extensively described in [7]. A model which enables analysis of convective instabilities was developed in [2] by separating mushy layer from the liquid region above and the solid beneath by fixing its thickness. It has been proved that convective instability in the mushy layer is generally subcritically unstable.

In the presence of multiple diffusive fields convection may arise even though fluid is statically stably stratified, i.e. the fluid density decreases with height. This phenomenon is called double-diffusive convection and originates due to a difference in diffusivities of various fields and is described in [21]. This feature is not present in binary mushy layer systems due to a coupling of thermal and solutal fields through the liquidus constraint. However, in ternary (or multicomponent) solidifying systems double diffusive effects may arise.

To identify the type of convective instability, a single primary mush model was studied in [3], [11]. Under a parametric reduction, namely zero speed of macroscopic solidification, zero Stefan number and by omitting solute segregation effects, linear stability problem associated to base state solution was analytically solved.

In [10] the stability of a primary mushy layer during the directional solidification of a ternary alloy is analysed. They developed a primary mush model, which contains phase-change effects due to latent-heat release, solute rejection and background solidification, which were not considered in the analytically solved model from [3]. The model identifies novel convective instabilities, both direct and oscillatory, which are present under statically stable conditions. An asymptotic analysis was carried out with respect to small thickness of primary mush with small growth rates.

In chapter §3, which is an extension of [13] (the original contribution of the author of this thesis) we consider directional solidification of ternary mixtures, incorporating thermal and solutal diffusion, segregation effects and finite speed of the background solidification. Apart from the boundary conditions prescribing constant concentrations on the top and the bottom of the primary mush, we also consider a boundary condition setup with fixed concentration gradients at the bottom. We present analytical solutions for the steady non-

convecting state, building on the results from [12], which consider the Lewis numbers and the segregation coefficients equal for both solutes.

2 Solidification and flow of a binary alloy over a moving substrate

The material in this section is based on our paper [15].

2.1 Model formulation

The region $x^* > 0$, $z^* > 0$ is filled with a binary alloy with the temperature and solute concentration T^*_∞ and C^*_∞ as $z^* \to \infty$, respectively. The solidification occurs from the cooled substrate $z^* = 0$, which moves horizontally at a constant speed $U^*_0 > 0$. The substrate is maintained the temperature $T^*_L(C^*_0)$, which by liquidus constraint corresponds to a concentration C^*_0. We assume that $T^*_L(C^*_0)$ is above the eutectic temperature T^*_E and below $T^*_L(C^*_\infty)$. We consider a situation where the binary-alloy mushy region forms between solid and liquid regions. We denote positions of the solid–mush and the mush–liquid interfaces as $z^* = a^*(x^*)$ and $z^* = b^*(x^*)$, respectively. We denote the local volume fraction of solid phase as ϕ. The situation described above is illustrated in figure 1.

The governing equations for temperature, concentration and solid fraction fields in the mushy layer are based on local conservation laws of heat and solute derived in [19].

We denote the flow velocity as $\boldsymbol{u}^* = (u^*, w^*)$ in the liquid and mushy regions, and the velocity of the solid phase as $\boldsymbol{v}^* = U^*_0\hat{\boldsymbol{i}}$, where $\hat{\boldsymbol{i}}$ is unit vector in horizontal direction. In the mush, the velocity field is $\boldsymbol{u}^* = \boldsymbol{v}^*$. We assume that there is no mass diffusion in the solid and that the solid is free of solute. Then the liquidus constraint in the takes the form

$$T^*_L\left(C^*\right) = T^*_L\left(C^*_0\right) - \Gamma^*\left(C^* - C^*_0\right). \tag{1}$$

2.2 Non-dimensionalisation

The lengths are scaled by a factor κ^*/U^*_0, and velocities by U^*_0. The dimensionless temperature and concentration are defined as

$$T = \frac{T^* - T^*_L(C^*_0)}{\Delta T^*} \qquad \text{and} \qquad C = \frac{C^*_0 - C^*}{\Delta C^*} \tag{2}$$

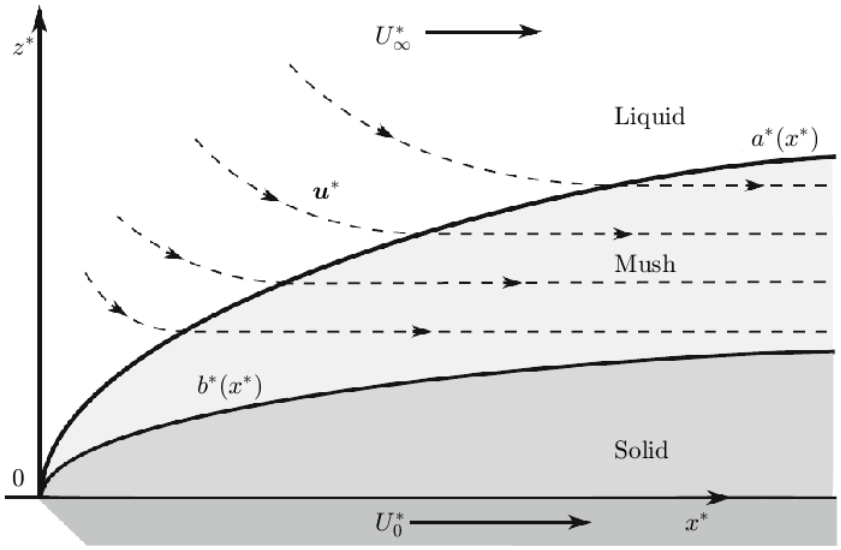

Figure 1: A sketch for the geometry of the solidification of a binary alloy over a horizontally moving substrate.

respectively, where $\Delta T^* = T^*_\infty - T^*_L(C^*_0)$ and $\Delta C^* = C^*_0 - C^*_\infty$. The non-dimensional positions of interfaces have the form

$$a\,(x) = \frac{a^*\,(\kappa^* x/U^*_0)}{\kappa^*/U^*_0} \qquad \text{and} \qquad b\,(x) = \frac{b^*\,(\kappa^* x/U^*_0)}{\kappa^*/U^*_0}. \tag{3}$$

The dimensionless numbers characterizing process of solidification are the Lewis number Le, the Stefan number S, the concentration ratio $\mathcal{C}$ and the dimensionless liquidus slope Γ defined respectively, by

$$Le = \frac{\kappa^*}{D^*}, \quad S = \frac{L^*_v}{c^*\Delta T^*}, \quad \mathcal{C} = \frac{C^*_0}{\Delta C^*}, \quad \Gamma = \frac{\Gamma^*\Delta C^*}{\Delta T^*}. \tag{4}$$

Note that range of $\mathcal{C}$ is $(1, \infty)$ and range of Γ is $(0, 1)$. The dimensionless numbers in the liquid are the Prandtl Pr number and the velocity ratio $\mathcal{U}$

$$Pr = \frac{\mu^*}{\kappa^*} \qquad \text{and} \qquad \mathcal{U} = \frac{U^*_\infty}{U^*_0}. \tag{5}$$

The resulting system of boundary-layer equations has the form:

$$T = 1,\, C = 1,\, u = \mathcal{U} \qquad \text{as} \qquad z \to \infty. \tag{6}$$

In the liquid phase ($z > b$):

$$u\frac{\partial u}{\partial x} + w\frac{\partial u}{\partial z} = Pr\frac{\partial^2 u}{\partial z^2}, \tag{7a}$$

$$u\frac{\partial T}{\partial x} + w\frac{\partial T}{\partial z} = \frac{\partial^2 T}{\partial z^2}, \tag{7b}$$

$$u\frac{\partial C}{\partial x} + w\frac{\partial C}{\partial z} = \frac{1}{Le}\frac{\partial^2 C}{\partial z^2}, \tag{7c}$$

$$\frac{\partial u}{\partial x} + \frac{\partial w}{\partial z} = 0. \tag{7d}$$

At mush–liquid interface ($z = b$):

$$S\frac{db}{dx}\phi_{b^-} = \left[\frac{\partial T}{\partial z}\right]_{b^+}^{b^-}, \tag{8a}$$

$$\frac{db}{dx}\left(\mathcal{C} - C\right)\phi_{b^-} = \frac{1}{Le}\left[(1-\phi)\frac{\partial C}{\partial z}\right]_{b^-}^{b^+}, \tag{8b}$$

$$\left[\frac{\partial T}{\partial x} + \frac{db}{dx}\,\frac{\partial T}{\partial z}\right]\Bigg|_{b^+} = \Gamma\left[\frac{\partial C}{\partial x} + \frac{db}{dx}\,s\frac{\partial C}{\partial z}\right]\Bigg|_{b^+}, \tag{8c}$$

$$T = \Gamma C,\; u = 1,\; w = 0. \tag{8d}$$

In the mush ($a < z < b$):

$$\frac{\partial T}{\partial x} = \frac{\partial^2 T}{\partial z^2} + S\frac{\partial \phi}{\partial x}, \tag{9a}$$

$$\frac{\partial}{\partial x}\left[(1-\phi)\left(C - \mathcal{C}\right)\right] = \frac{1}{Le}\frac{\partial}{\partial z}\left[(1-\phi)\,\frac{\partial C}{\partial z}\right], \tag{9b}$$

$$T = \Gamma C. \tag{9c}$$

At mush–solid Interface ($z = a$):

$$S\frac{da}{dx}\left(1 - \phi_{a^+}\right) = \left[\frac{\partial T}{\partial z}\right]_{a^+}^{a^-}, \tag{10a}$$

$$\frac{da}{dx}\left(\mathcal{C} - C\right)\left(1 - \phi_{a^+}\right) = \frac{1}{Le}(1-\phi)\,\frac{\partial C}{\partial z}\Bigg|_{a^+}, \tag{10b}$$

$$T|_{a^+} = \Gamma\, C|_{a^+}\,. \tag{10c}$$

In the solid phase ($0 < z < a$):

$$\frac{\partial T}{\partial x} = \frac{\partial^2 T}{\partial z^2}. \tag{11}$$

At the bottom,

$$T = 0 \qquad \text{at} \qquad z = 0. \tag{12}$$

2.3 Self-similar reduction

Velocity field can be described using the stream function ψ defined by

$$u = \frac{\partial \psi}{\partial z}, \quad w = -\frac{\partial \psi}{\partial x}. \tag{13}$$

We seek a self-similar solution of the form:

$$\psi(x,z) = 2x^{1/2} f(\xi), \text{ where } \qquad \xi = \frac{z}{2\sqrt{x}} = O(1) \qquad \text{as} \qquad Pr \to 0, \tag{14}$$

with the positions of dimensionless interfaces given as

$$a(x) = 2\lambda_a x^{1/2} \qquad \text{and} \qquad b(x) = 2\lambda_b x^{1/2}, \tag{15}$$

where λ_a and λ_b are constants yet to be determined and f satisfies the boundary value problem described in [16] and [14].

2.4 Results for small Pr limit

As $Pr \to 0$ the velocity, temperature and concentration fields, in the liquid are

$$u \sim 1 + (1-\mathcal{U}) \left[\exp\left(-2\lambda_b \frac{\xi - \lambda_b}{Pr} \right) - 1 \right], \tag{16a}$$

$$w \sim -\frac{1-\mathcal{U}}{x^{1/2}} \left[\lambda_b + \frac{Pr}{2\lambda_b} - \left(\xi + \frac{Pr}{2\lambda_b} \right) \exp\left(-2\lambda_b \frac{\xi - \lambda_b}{Pr} \right) \right], \tag{16b}$$

$$T \sim 1 + (T_b - 1) \frac{\operatorname{erfc}\left[\mathcal{U}^{1/2} (\xi - \lambda_b) + \mathcal{U}^{-1/2} \Lambda(\lambda_b) \right]}{\operatorname{erfc}\left[\mathcal{U}^{-1/2} \Lambda(\lambda_b) \right]}, \tag{16c}$$

$$C \sim 1 + (C_b - 1) \frac{\operatorname{erfc}\left[(\mathcal{U} Le)^{1/2} (\xi - \lambda_b) + (\mathcal{U}/Le)^{-1/2} \Lambda(\lambda_b) \right]}{\operatorname{erfc}\left[(\mathcal{U}/Le)^{-1/2} \Lambda(\lambda_b) \right]}, \tag{16d}$$

where

$$\operatorname{erfc} = 1 - \operatorname{erf}(\xi), \quad \operatorname{erf}(\xi) = \frac{2}{\sqrt{\pi}} \int_0^\xi \mathrm{e}^{-s^2} \mathrm{d}s \text{ and } \Lambda(\lambda_b) = \lambda_b + Pr \frac{1-\mathcal{U}}{2\lambda_b}. \tag{17}$$

Dimensionless amount of solute contained in mushy layer is expressed as

$$\int_{\lambda_a}^{\lambda_b} (\mathcal{C} - C)(1-\phi) \, \mathrm{d}s = \frac{1}{2} \left[2\lambda_b (\mathcal{C} - C_b) - \frac{1}{Le} C'_{b^-} \right] (1 - \phi_{b^-}). \tag{18}$$

For general value of S was shown that the concentration gradient is continuous across the mush–liquid interface $C'_{b^+} = C'_{b^-}$ and that $\phi_{b^-} = 0$.

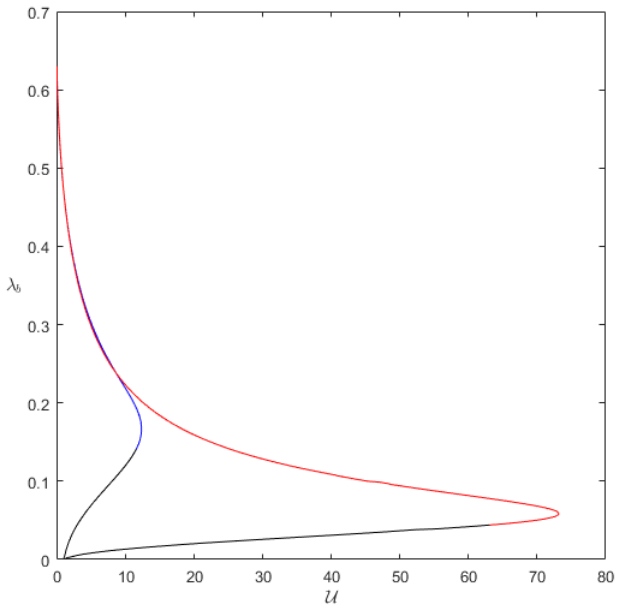

Figure 2: The position of the mush–liquid interface λ_b, as function of the velocity ratio $\mathcal{U}$ computed from (19b). The red curve correspods to $Pr = 10^{-3}$ and the blue curve corresponds to $Pr = 10^{-2}$. The black portions correspond to the case when criterion $Pr/\lambda_b^2 > 0.5$. The values of other parameters used are $Le = 100$ and $\Gamma = 0.5$.

2.5 Asymptotic results with no latent heat release

The problem is solved analytically up to the pair of algebraic equations exhibiting only solidification rates constants λ_a and λ_b:

$$LeG\left(\lambda_a\right)\left[C_b - \mathcal{C}\frac{\operatorname{erf}\left(\lambda_b\right)}{\operatorname{erf}\left(\lambda_a\right)}\right] + C_b = 0, \tag{19a}$$

$$\frac{\lambda_b}{Le}F\left[\frac{\Lambda\left(\lambda_b\right)}{\sqrt{\mathcal{U}/Le}}\right] - \Gamma\lambda_b F\left[\frac{\Lambda\left(\lambda_b\right)}{\sqrt{\mathcal{U}}}\right] + \left(1-\Gamma\right)\Lambda\left(\lambda_b\right)G\left(\lambda_b\right) = 0, \tag{19b}$$

where

$$F\left(\lambda\right) = \sqrt{\pi}\lambda \mathrm{e}^{\lambda^2}\operatorname{erfc}\left(\lambda\right) \text{ and } G\left(\lambda\right) = \sqrt{\pi}\lambda \mathrm{e}^{\lambda^2}\operatorname{erf}\left(\lambda\right). \tag{20}$$

The temperature and concentration values at the mush–liquid interface

$$T_b = 1 - \frac{\lambda_b F\left[\Lambda\left(\lambda_b\right)/\sqrt{\mathcal{U}}\right]}{\lambda_b F\left[\Lambda\left(\lambda_b\right)/\sqrt{\mathcal{U}}\right] + \Lambda\left(\lambda_b\right) G\left(\lambda_b\right)}, \tag{21a}$$

$$C_b = 1 - \frac{\lambda_b F\left[\Lambda\left(\lambda_b\right)/\sqrt{\mathcal{U}/Le}\right]}{\lambda_b F\left[\Lambda\left(\lambda_b\right)/\sqrt{\mathcal{U}/Le}\right] + Le\Lambda\left(\lambda_b\right) G\left(\lambda_b\right)}. \tag{21b}$$

Using (21b) and (19b), the dependence of C_b and λ_b on Pr, Γ, Le and $\mathcal{U}$ was examined. Notably, the independence of C_b and λ_b on Pr, the almost linear dependence of λ_b on Γ and the transition to the small diffusivity limit as $Le \to \infty$.

In the limit $Le \to \infty$, a concentration boundary layer of thickness $O(Le^{-1/2})$ forms ahead of the mush–liquid interface. Since $F(s) \sim 1$ and $G(s) \sim s\mathrm{e}^{s^2}$ as $s \to \infty$, the only admissible solution of (19b) is of unit order. The solution of (19a) is

$$\lambda_a = \frac{1/Le}{\pi^{1/2}\mathcal{C}\mathrm{erf}\left(\lambda_b\right)} + O\left(Le^{-2}\right) \qquad \text{as} \qquad Le \to \infty. \tag{22}$$

Observe that λ_b, in (19b), does not depend on the concentration ratio $\mathcal{C}$, so that the thickness of the solid decreases with $\mathcal{C}$. The case $\mathcal{U} = 0$ corresponds to the far-field velocity U_∞^* set to zero. The growth rates λ_a and λ_b are independent of U_0^* and hence the dimensional position of interfaces

$$a^*\left(x^*\right) = 2\lambda_a\left(\kappa^* x^*/U_0^*\right)^{1/2}, \quad b^*\left(x^*\right) = 2\lambda_b\left(\kappa^* x^*/U_0^*\right)^{1/2},$$

is proportional to the $(U_0^*)^{-1/2}$. The temperature and concentration fields in the liquid phase can be expressed as

$$T \sim 1 - Le\frac{1-\Gamma}{Le-1}\exp\left[-\frac{2\lambda_b^2 + Pr}{\lambda_b}\left(\xi - \lambda_b\right)\right], \tag{23a}$$

$$C \sim 1 - \frac{1-\Gamma}{(Le-1)\,\Gamma}\exp\left[-Le\frac{2\lambda_b^2 + Pr}{\lambda_b}\left(\xi - \lambda_b\right)\right]. \tag{23b}$$

Equation (19a) is unchanged, while equation for the growth constant λ_b satisfies the algebraic equation

$$G\left(\lambda_b\right)\left(1 + \frac{Pr}{2\lambda_b^2}\right) = \frac{\Gamma - 1/Le}{1-\Gamma}. \tag{24}$$

A positive solution of (24) exists only if $\Gamma Le > 1$. By computing a derivative of implicitly defined function (24) we find that λ_b increases with Γ and Le, and decreases with Pr.

3 Steady states in ternary alloy solidification

The material in this section is based on our paper [13].

3.1 Model formulation

The isolated primary mush of the ternary alloy was considered, following the models [3], [10] and [11]. We consider four different types of boundary conditions (BCs), which combine fixed concentrations and fixed solutal fluxes denoted by C and F respectively: C–C, F–C, C–F and F–F. For all boundary condition types, a unified form of dimensionless governing equations was identified. Different BC types are reflected in the definitions of dimensionless parameters. Following [3], the lengths are scaled by the height of mushy layer, denoted as H^*, time by H^{*2}/κ_l^*, where $\kappa_l^* = k_l^*/c_l^*$ is the thermal diffusivity, and velocity by κ_l^*/H^*.

For brevity, we present here only the non-dimensionalisation employed for C–C type of BCs. The non-dimensional temperature and concentrations are defined as

$$T = \frac{T^* - T_M^{3*}}{T_{top}^* - T_{bot}^*}, \quad C_j = \frac{C_j^*}{C_{jtop}^* - C_{jbot}^*}. \tag{25}$$

A set of dimensionless parameters is

$$V = \frac{V^* H^*}{\kappa_l^*}, \quad S = \frac{L_v^*}{c_l^* \left(T_{top}^* - T_{bot}^*\right)}, \quad Le_j = \frac{\kappa_l^*}{D_j^*}, \quad m_j = \frac{m_j^* \left(C_{jtop}^* - C_{jbot}^*\right)}{\left(T_{top}^* - T_{bot}^*\right)}.$$

These definitions lead to the dimensionless BCs

$$T = T_{bot} + 1,\, C_1 = C_{1bot} + 1,\, C_2 = C_{2bot} + 1,\, \phi = \phi_0,\, \boldsymbol{u} \cdot \hat{\boldsymbol{k}} = 0 \text{ at } z = 1$$

$$\text{and } T = T_{bot},\, C_1 = C_{1bot},\, C_2 = C_{2bot},\, \boldsymbol{u} \cdot \hat{\boldsymbol{k}} = 0 \text{ at } z = 0$$

and the coupling $T_{bot} = m_1 C_{1bot} + m_2 C_{2bot}$, where

$$C_{jbot} = \frac{C_{jbot}^*}{C_{jtop}^* - C_{jbot}^*}, \quad C_{jtop} = \frac{C_{jtop}^*}{C_{jtop}^* - C_{jbot}^*} \quad \text{and } T_{bot} = \frac{T_{bot}^* - T_M^{3*}}{T_{top}^* - T_{bot}^*}. \tag{26}$$

Note that $T_{bot} \in (-\infty; -1)$.

3.2 Analytical base-state solutions

A steady one-dimensional solution without convection as is denoted a base state solution. The analytical solutions are presented for the case in which both statically–stably and

statically unstably stratified concentration profiles are present, allowing further study of doubly-diffusing convection in statically–stable region described in [3]. The same speed of solute rejection $k_1 = k_2 \equiv k$, the same Lewis numbers $Le_1 = Le_2 = Le$ and zero Stefan number $S = 0$ are assumed. The same material properties of the liquid and solid phases, namely thermal conductivity $k_s^* = k_l^*$ and specific heat $c_s^* = c_l^*$ are assumed. The most important features of presented solutions are finite speed of macroscopic solidification ($V \neq 0$) and presence of partial solute rejection effects ($k \neq 1$).

The system of equations governing the base state has the form:

$$-V\frac{\mathrm{d}\bar{T}}{\mathrm{d}z} = \frac{\mathrm{d}^2\bar{T}}{\mathrm{d}z^2}, \tag{27a}$$

$$-V\left(1-\bar{\phi}\right)\frac{\mathrm{d}\bar{C}_j}{\mathrm{d}z} = \frac{1}{Le}\frac{\mathrm{d}}{\mathrm{d}z}\left[\left(1-\bar{\phi}\right)\frac{\mathrm{d}\bar{C}_j}{\mathrm{d}z}\right] - V\left(1-k\right)\bar{C}_j\frac{\mathrm{d}\bar{\phi}}{\mathrm{d}z}, \quad \text{for } j=1,2, \tag{27b}$$

$$\bar{T} = m_1\bar{C}_1 + m_2\bar{C}_2, \tag{27c}$$

with one of the BCs types:

$$\begin{aligned}
&\text{C–C}: \quad \bar{C}_j\left(0\right) = C_{jbot}, \quad \bar{C}_j\left(1\right) = C_{jbot}+1, \quad \bar{\phi}\left(1\right) = \phi_0;\\
&\text{F–C}: \quad \frac{\mathrm{d}\bar{C}_j}{\mathrm{d}z}\left(0\right) = 1, \quad \bar{C}_j\left(1\right) = C_{jtop}, \quad \bar{\phi}\left(1\right) = \phi_0;\\
&\text{C–F}: \quad \bar{C}_j\left(0\right) = C_{jbot}, \quad \frac{\mathrm{d}\bar{C}_j}{\mathrm{d}z}\left(1\right) = 1, \quad \bar{\phi}\left(1\right) = \phi_0;\\
&\text{F–F}: \quad \bar{C}_j\left(0\right) = C_{jbot}, \quad \frac{\mathrm{d}\bar{C}_j}{\mathrm{d}z}\left(0\right) = 1, \quad \frac{\mathrm{d}\bar{C}_j}{\mathrm{d}z}\left(1\right) = G_j, \quad \bar{\phi}\left(1\right) = \phi_0.
\end{aligned}$$

The concentrations profiles satisfy

$$\frac{\mathrm{d}^2\bar{C}_j}{\mathrm{d}z^2} + \left[\frac{\mathrm{d}}{\mathrm{d}z}\ln\left(1-\bar{\phi}\right) + LeV\right]\frac{\mathrm{d}\bar{C}_j}{\mathrm{d}z} + \left[VLe\left(1-k\right)\frac{\mathrm{d}}{\mathrm{d}z}\ln\left(1-\bar{\phi}\right)\right]\bar{C}_j = 0. \tag{28}$$

This equation can be transformed to a hypergeometric equation

$$\frac{\mathrm{d}^2\bar{C}_j}{\mathrm{d}\xi^2}\xi\left(1-\xi\right) + \frac{\mathrm{d}\bar{C}_j}{\mathrm{d}\xi}\left[c-\xi\left(1+a+b\right)\right] - ab\bar{C}_j = 0, \tag{29}$$

where $a=-1$, $b=-\frac{Le(1-k)}{\eta}$, $c=-\frac{1}{\eta}$, $\eta=\frac{(1-k)-1/Le}{1-1/Le}$ and

$$\xi\left(z\right) = 1 - \frac{\left(Le-1\right)\eta}{Le\left(1-k\right)\delta}\mathrm{e}^{-Vz} \text{ and } \delta = \frac{\mathrm{e}^{-V}\bar{T}\left(0\right)-\bar{T}\left(1\right)}{\bar{T}\left(1\right)-\bar{T}\left(0\right)}. \tag{30}$$

Note that (29) is a linear second-order differential equation with three regular singular points. The solution of the system (27) has the form:

$$\bar{\phi}(z) = 1 - (1-\phi_0)\left(\xi(1)/\xi(z)\right)^{\frac{1}{\eta}}, \tag{31a}$$

$$\bar{C}_j(z) = \alpha_j w_{1(x)}(z) + \beta_j w_{2(x)}(z) \text{ for } j = 1, 2, \tag{31b}$$

where $w_{i(x)}$ refers to the i-th independent solution around $\xi = x$. Their form is determined by regime of ξ, defined by the values of V, Le, k and T_{bot} (or T_{top}).

The solutions within different parametric regimes were obtained by considering expansions around different regular singular points.

3.3 Asymptotic results for $Le \to \infty$ in C–C case

The leading-order asymptotic expansion of (31) for $1 < -T_{bot} < 1/\left(1 - \mathrm{e}^{-V}\right)$, takes the form

$$\bar{\phi}(z) = 1 - (1-\phi_0)\left(\frac{\xi(z)}{\xi(1)}\right)^{-\frac{1}{1-k}} + O(1/Le), \tag{32}$$

$$\bar{C}_j(z) = \frac{C_{jbot}+1}{T_{bot}+1}\bar{T}(z) + \frac{C_{jbot}-T_{bot}}{T_{bot}+1}\vartheta(z) + O(1/Le), \text{ for } j = 1, 2. \tag{33}$$

where

$$\vartheta(z) = \left(\frac{\xi(z)}{\xi(0)}\right)^{k/(1-k)} \mathrm{e}^{-VLez}. \tag{34}$$

The formulae analogous to (33) in the regime $-T_{bot} > 1/\left(1 - \mathrm{e}^{-V}\right)$, are

$$\bar{C}_j(z) = C_{jbot}\frac{\xi(z)}{\xi(1)} + \vartheta(z)\left(\frac{\xi(z)}{\xi(0)}\right)^{-\frac{2}{1-k}}\left[C_{jbot} - (C_{jbot}+1)\frac{\xi(z)}{\xi(1)}\right] + O(1/Le) \text{ for } j = 1, 2. \tag{35}$$

The second term of (33) vanishes as $|C_{1bot} - C_{2bot}|$ is small, in that case the first term dictates concentration profiles to be proportional to $\bar{T}$ and hence monotonic. Therefore non-monotonicity of concentration profile can occur only when difference $|C_{1bot} - C_{2bot}|$ exceeds some threshold. In figure 3 the analytical solution with the leading-order solution (32) are compared.

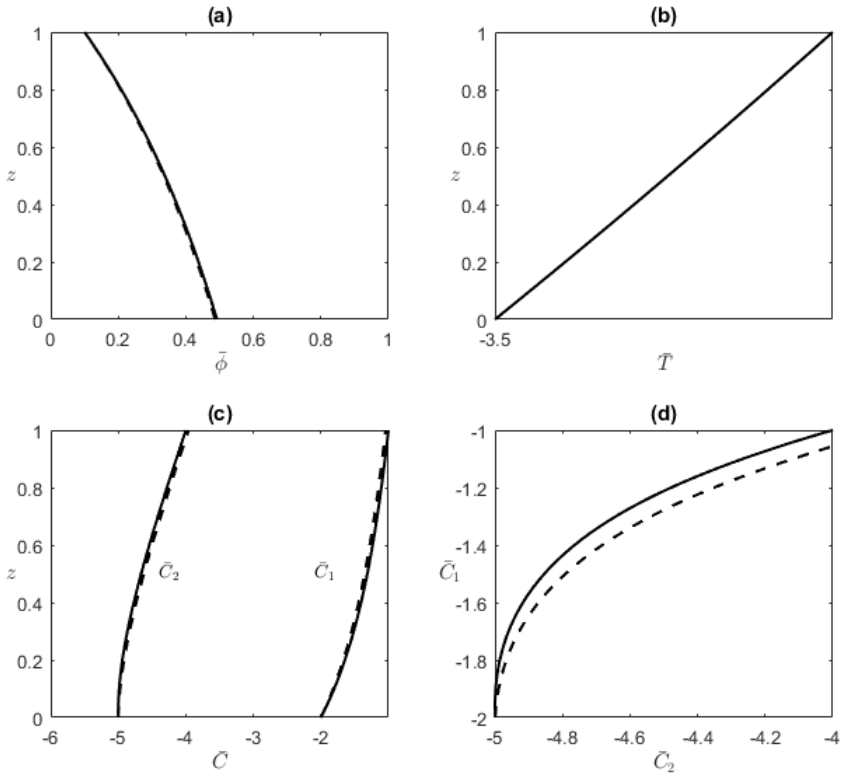

Figure 3: Comparison of the explicit solution calculated from (31) and C–C type BCs (solid) and the leading-order asymptotic solution (32) (dashed) in the regime of $\xi < 0$. Parameter values used here are $m_1 = m_2 = 0.5$, $Le_1 = Le_2 = 25$, $k_1 = k_2 = 0.3$, $k_s/k_l = 1$, $c_s/c_l = 1$, $S = 0$, $V = 0.1$. The BCs are $C_{1bot} = -2$, $C_{2bot} = -5$ and $\phi_0 = 0.1$.

3.4 Asymptotic results for $C_{1bot} \to -\infty$

The limit $C_{1bot} \to -\infty$ with $C_{2bot} = O(1)$ was considered. By swapping the solutal indices the results for the limit $C_{2bot} \to -\infty$ with $C_{1bot} = O(1)$ can be obtained.

For large values of C_{1bot}, the scaled coordinate is $\xi = 1 + O(1/C_{1bot})$, therefore the expansion around regular singular point $\xi = 1$ of (29) is employed.

For $\phi(z)$, $\bar{C}_1(z)$ and $\bar{C}_2(z)$ we have

$$\bar{\phi}(z) = \phi_0 + \frac{1}{m_1 C_{1bot}} \frac{(1-\phi_0)(Le-1)}{(1-k)\,Le} \frac{\mathrm{e}^{-V} - \mathrm{e}^{-Vz}}{1-\mathrm{e}^{-V}} + O(1/C_{1bot}^2), \tag{36a}$$

$$\bar{C}_1(z) = C_{1bot} - \frac{m_2}{m_1} \frac{1-\mathrm{e}^{-LeVz}}{1-\mathrm{e}^{-LeV}} + \frac{1}{m_1} \frac{1-\mathrm{e}^{-Vz}}{1-\mathrm{e}^{-V}} + O(1/C_{1bot}), \tag{36b}$$

$$\bar{C}_2(z) = C_{2bot} + \frac{1-\mathrm{e}^{-LeVz}}{1-\mathrm{e}^{-LeV}} + O(1/C_{1bot}). \tag{36c}$$

3.5 Static stability: Parametric dependence

The base state is statically stably stratified if density of fluid is decreasing function of z, therefore non-monotonic behaviour of concentration profile can induce statically unstable situation.

In C–C case the non-monotonic behaviour of concentration profiles is a function of BCs:

$$C_{1bot} = \frac{T_{bot}\Omega - 1}{1+\Omega}, \quad C_{2bot} = \frac{T_{bot}\Omega - 1}{1+\Omega}, \tag{37}$$

where $\Omega := \left(1-\mathrm{e}^{-V}\right)\left[\frac{k(Le-1/(1-k))}{Le(1-k)T_{bot}(1-\mathrm{e}^{-V})+1} - Le\right]$. In figure 4, three qualitatively different scenarios are depicted: (a) profile of $\bar{C}_2$ is non-monotonic; (b) both concentration profiles are monotonic and (c) profile of $\bar{C}_1$ is non-monotonic.

4 Summary

In this thesis, two problems involving solidification have been studied. The first is the solidification of a binary alloy pulled horizontally, and the second is the solidification of a ternary alloy in vertically moving frame of reference.

The §2 considering the solidification of a binary alloy over a horizontally moving substrate is based on [15]. The results obtained can be compared to [14], where the mushy layer is absent, but the geometry of the problem is similar. The dimensional thickness of the solid phase was proportional to $U_\infty^{*1/2}/U_0^*$, provided $Pr \ll \mathcal{U}$, in contrast to the present case where the dimensional thickness is proportional to $1/U_0^{*1/2}$. The dependence of λ_b and C_b on the non-dimensional parameters Pr, $\mathcal{U}$, Le and Γ evaluated from (21b) and (19b) respectively have been shown. Notable is the independence of concentration and the mushy layer thickness on Pr, the fact that the mushy layer thickness is an increasing function of

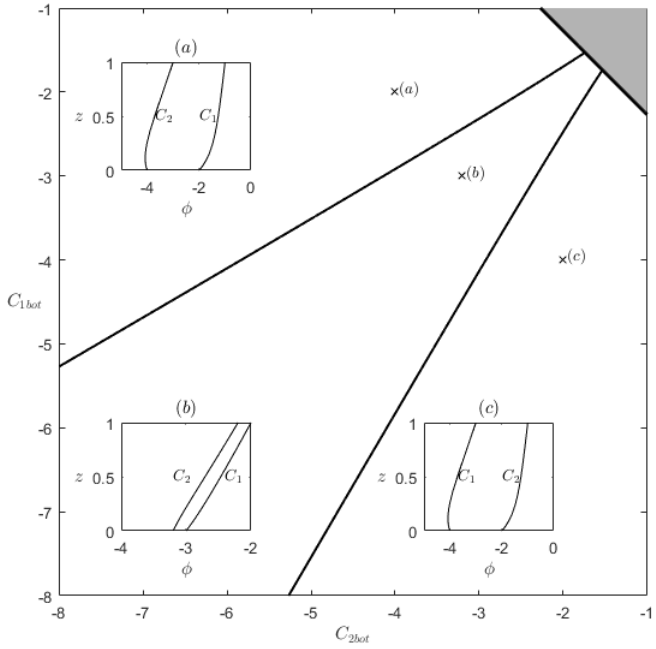

Figure 4: The classification of compositional profiles in dependence on concentration BC in the C_{2bot} vs. C_{1bot} plane. Lines along which the profiles change their monotonic behaviour were determined using asymptotic result (37). In the grey region at the top right corner the model is not physically meaningful. Three qualitatively different scenarios are depicted with BC as shown. Parameters used were $Le = 50$, $k = 0.7$, $V = 0.1$, $\phi_0 = 0.1$ and $m_1 = 0.5$.

Γ and Le, and the transition of the interfacial concentration and interface position to the small diffusivity limit as $Le \to \infty$. For $\mathcal{U} = 0$, we have shown that λ_b is an increasing function of both Γ and Le.

In §3 was analysed the model of directional solidification in the primary mushy layer studied also in [3], [10] and [11]. A number of different types of boundary conditions have been introduced, namely F–C, C–F and F–F, where C or F refer to the solute concentration or solutal flux fixed at the boundary. In contrast to [10], a finite pulling speed was considered. The explicit solutions for the base state in terms of hypergeometric functions have been identified. In figure 4 the presented asymptotic results are compared to the numerical results of [3]. The region (grey) shows, where the model is not physically meaningful was

identified. Depending on the solutal expansion coefficients, the results from §3.5 identify the critical curves of static stability in the parameter space of C_{1bot} vs. C_{2bot}. We show that the critical lines are in general non-linear and that in this case approach the oblique asymptote as $Le \to \infty$.

References

[1] Aharonov, E., Spiegelman, M., Kelemen, P., *Three-dimensional flow and reaction in porous media: Implications for the Earth's mantle and sedimentary basins*, J. Geophys. Res. Solid. Earth **102** (B7) (1997), 14821–14833.

[2] Amberg, G., Homsy, G.M., *Nonlinear analysis of buoyant convection in binary solidification with application to channel formation*, J. Fluid Mech. **252** (1993), 79–98.

[3] Anderson, D. M., McFadden, G. B., Coriell, S. R., & Murray, B. T., *Convective instabilities during the solidification of an ideal ternary alloy in a mushy layer*, J. Fluid Mech. **647** (2010), 309–333.

[4] Anderson, D. M., Guba, P., *Convective phenomena in mushy layers*, under review.

[5] Carolsfeld, J., Godinho, H. P., Zaniboni Filho, E., Harvey, B.J., *Cryopreservation of sperm in Brazilian migratory fish conservation*, J. Fish Biol. **63**(2) (2003), 472–489.

[6] Dahle, A. K., StJohn, D. H., *Rheological behaviour of the mushy zone and its effect on the formation of casting defects during solidification*, Acta Mater. **47** (1) (1998), 31–41.

[7] Davis, S. H., *Theory of solidification*, (2001), Cambridge University Press.

[8] Fearn, D. R., *Hydromagnetic flow in planetary cores*, Rep. Prog. Phys., **61** (3) (1998), 175–235.

[9] Galdi, G. P., Payne, L. E., Proctor, M. R. E., Straughan, B., *Convection in thawing subsea permafrost*, Proc. R. Soc. Lond. A, **414** (1846) (1987), 83–102.

[10] Guba, P., Anderson, D. M., *Diffusive and phase change instabilities in a ternary mushy layer*, J. Fluid Mech. **760** (2014), 634–669.

[11] Guba, P., Anderson, D. M., *Pattern selection in ternary mushy layers*, J. Fluid Mech. **825** (2017), 853–886.

[12] Hurban, M., *Static stability of three-component systems*, Master's thesis (2015), Comenius University, Bratislava, Slovakia.

[13] Hurban, M., *Steady non-convection states in ternary alloy solidification*, under review, (2019).

[14] Kyselica, J., Guba, P., *Forced flow and solidification over a moving substrate*, Appl. Math. Model. **40** (1) (2016), 31–40.

[15] Kyselica, J., Guba, P., Hurban, M., *Solidification and flow of a binary alloy over a moving substrate*, Transp. Porous Media **121** (2) (2018), 419-435.

[16] Löfgren, H. B., *Ideal solidification of a liquid-metal boundary layer flow over a conveying substrate*, J. Fluid Mech. **446** (2001), 121–131.

[17] Mullins, W., Sekerka, R. F., *Stability of a planar interface during solidification of a dilute binary alloy*, J. Appl. Phys. **35** (2) (1964), 444–451.

[18] Ruddick, B., Gargett, A. E., *Oceanic double-diffusion: introduction*, Prog. Oceanogr. **56** (2003), 381–393.

[19] Schulze, T. P., Worster, M. G., *A time-dependent formulation of the mushy-zone free-boundary problem*, J. Fluid Mech. **541** (2005), 193–202.

[20] Tangthieng, C., Cheung, F. B., Shiah, S. W., *Behavior of the two-phase mushy zone during freeze coating on a continuous moving plate*, J. Heat Transfer **124** (2002), 111-119.

[21] Turner, J. S., *Double-Diffusive Phenomena*, Annu. Rev. Fluid Mech. **6** (1) (1974), 37–54.

[22] Worster, M. G., *Solidification of an alloy from a cooled boundary*, J. Fluid Mech. **167** (1986), 481–501.

[23] Worster, M. G., *Convection in mushy layers*, Annu Rev Fluid Mech, **29** (1) (1997), 91–122.

List of publications

1. Hurban, M., *Steady non-convection states in ternary alloy solidification*, under review, (2019).

2. Kyselica, J., Guba, P., Hurban, M., *Solidification and flow of a binary alloy over a moving substrate*, Transp. Porous Media, **121** (2) (2018), 419–435.

3. Hurban, M., *Dualita geometrického programovania a jej možné analógie*, Zborník príspevkovm, Študentská vedecká konferencia FMFI UK, Bratislava, (2014).

Grants

- Modelovanie viaczložkových systémov podliehajúcich fázovej premene (hlavný riešiteľ), Grant UK/343/2016

Teaching

- *Metódy voľne optimalizácie*, vedenie cvičení pre 2. ročník bakalárskeho odboru Ekonomická a finančná matematika, letný semester 2019.

- *Numerické metódy*, vedenie cvičení pre 3. ročník bakalárskeho odboru Ekonomická a finančná matematika, letné semestre 2016, 2017 a 2018.

- *Cvičenia z nelineárneho programovania*, vedenie cvičení pre 3. ročník bakalárskeho odboru Ekonomická a finančná matematika, zimné semestre 2015,2016,2017 a 2018.

Supervision of batchelor theses

- Kováč, L., Pravdepodobnostné modely v lukostreľbe, 2016

- Kostroš, M., Optimálna stratégia hry Super farmár, 2017

- Joščáková, V., Modelovanie a meranie výkonnosti lukostrelcov, 2017

- Šošovička, M., Modelovanie výkonnosti šachistov, 2018

- Havlíčková, P., Problém viacnásobných meraní – príklady, 2019